

Carboxylate Ion Pairing with Alkali-Metal Ions for β -Lactoglobulin and Its Role on Aggregation and Interfacial Adsorption

Frank R. Beierlein,^{†,‡} Timothy Clark,^{*,†,‡,||} Björn Braunschweig,^{‡,§} Kathrin Engelhardt,[§] Lena Glas,[§] and Wolfgang Peukert^{‡,§}

[†]Computer-Chemie-Centrum and Interdisciplinary Center for Molecular Materials, Friedrich-Alexander-Universität Erlangen-Nürnberg, Nägelsbachstr. 25, 91052 Erlangen, Germany

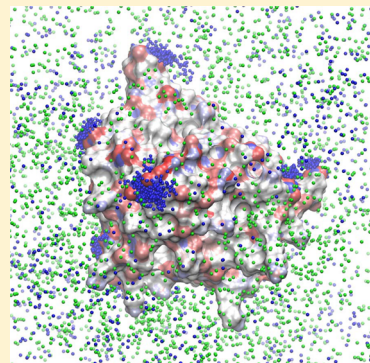
[‡]Cluster of Excellence Engineering of Advanced Materials, Friedrich-Alexander-Universität Erlangen-Nürnberg, Nägelsbachstr. 49b, 91052 Erlangen, Germany

^{*}Institute of Particle Technology (LFG), Friedrich-Alexander-Universität Erlangen-Nürnberg, Cauerstraße 4, 91058 Erlangen, Germany

^{||}Centre for Molecular Design, University of Portsmouth, King Henry Building, King Henry I Street, Portsmouth PO1 2DY, United Kingdom

Supporting Information

ABSTRACT: We report a combined experimental and computational study of the whey protein β -lactoglobulin (BLG) in different electrolyte solutions. Vibrational sum-frequency generation (SFG) and ellipsometry were used to investigate the molecular structure of BLG modified air–water interfaces as a function of LiCl, NaCl, and KCl concentrations. Molecular dynamics (MD) simulations and thermodynamic integration provided details of the ion pairing of protein surface residues with alkali-metal cations. Our results at pH 6.2 indicate that BLG at the air–water interface forms mono- and bilayers preferably at low and high ionic strength, respectively. Results from SFG spectroscopy and ellipsometry are consistent with intimate ion pairing of alkali-metal cations with aspartate and glutamate carboxylates, which is shown to be more effective for smaller cations (Li^+ and Na^+). MD simulations show not only carboxylate–alkali-metal ion pairs but also ion multiplets with the alkali-metal ion in a bridging position between two or more carboxylates. Consequently, alkali-metal cations can bridge carboxylates not only within a monomer but also between monomers, thus providing an important dimerization mechanism between hydrophilic surface patches.



INTRODUCTION

Medium effects such as solvation and ion pairing are instrumental in determining the structure,^{1,2} function, and reactivity³ of proteins and peptides. They therefore play an important role in processes such as protein crystallization,^{4,5} purification of pharmaceuticals by foam fractionation,^{6,7} or formulation of protein foams in food products.⁸ Counterions interact primarily with charged protein side chains but also directly with the protein backbone. Pairing of ions with functional groups can affect the interaction of not only protein but also colloidal particles in two main ways: In a first, rather simplistic view, attractive or repulsive Coulombic interactions between charged particles based on their net charges are considered, ignoring specific interaction between functional groups and ions. In this model, changing the apparent/net charge of the protein,² e.g., by (de)protonation or by complexation with different counterions, affects the intermolecular interactions and is used, e.g., to explain effects such as aggregation of proteins at interfaces. It is evident that protein–protein interactions result from local interactions of molecular groups predominantly located on the protein surface or from

hydrophobic effects. For this reason, it is of great importance to understand the driving forces and mechanisms of protein–protein interactions on an atomic level. Despite its importance, the latter information is not available for many systems. We now present a detailed study of such factors for β -lactoglobulin (BLG) as a role model for other proteins.

One area in which interprotein interactions are technically important is that of protein foams. As hierarchical materials, the macroscopic properties of foams are determined by the structure and intermolecular interaction within the ubiquitous air–water interfaces.^{9,10} Milk foams, which contain significant amounts of BLG, serve as an example.

The isoelectric point (IEP) of a mixture of BLG variants A (BLGA) and B (BLGB) in water, directly at the electrolyte–air interface, has been determined to be approximately 5.1.⁹ Previous studies of surface-adsorbed layers of bovine serum albumin (BSA),¹⁰ and BLG⁹ near the IEP, concluded that

Received: February 27, 2015

Revised: March 30, 2015

Published: March 31, 2015

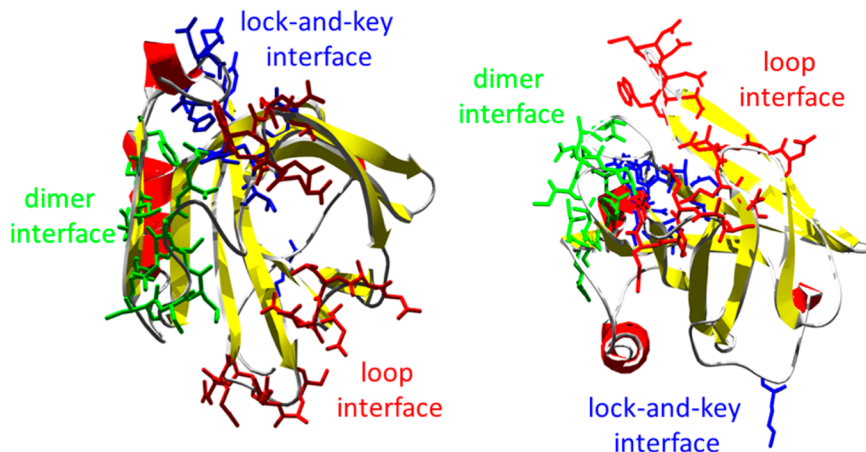


Figure 1. BLG monomer (cartoon representation) viewed from two different directions, with residues involved in the formation of different dimers as colored sticks (blue, “lock-and-key”; green, “dimer”; red, “loop interface”), based on PDB structure 3BLG.³⁶ Residues involved in contacts are “lock-and-key”: Lys8, Tyr20-Ser21, Val41-Glu44, Leu156-Glu158, His161; “loop”: Trp61-Ala67, Asp85-Asn90, Ser110-Gln115; “dimer interface”: Ile29-Gln35, Ile147-Phe151. Images were created using Swiss-PDB-Viewer³⁹ and Pov-Ray.⁴⁰

interfacial protein layers are uncharged, which results in attractive intermolecular interactions and the formation of thick agglomerated protein multilayers at the air–water interface. It has been argued based on a simple electrostatic approach that considers the net charge of the proteins that the interactions between charged protein molecules become repulsive at higher or lower pH values with respect to the IEP, leading to the formation of BLG monolayers and to polar ordered and highly polarized water molecules.^{9,10} However, simple net-charge-based models are not necessarily accurate. For instance, deprotonated polycarboxylate micelles with nominal charges of $-100e$ or larger have been found to attract each other in the presence of sodium counterions more strongly than the neutral species, which can form bridging hydrogen bonds.¹¹

Ion and salt effects on the solubility and aggregation properties of proteins have been known since the early work of Hofmeister.¹² Many attempts to rationalize Hofmeister’s observations have been reported in the succeeding 126 years,^{13,14} but no single interpretation exists that can explain all known salt effects.^{15–18} However, it has become clear that it is essential to study specific ion–biomolecule interactions, e.g., the pairing of ions from solution with charged and highly polar groups at the biomolecular surface.^{15,16} The surface chemistry of proteins is complex and represents an active field of research because of the importance of protein dimerization in biological signaling and misfolding diseases.¹⁹ Although hydrophobic residues are generally more prevalent than polar ones in dimerization surface patches, the latter are well represented, so that hydrogen bonding and salt bridges are also thought to be important.²⁰ This combination has been suggested to lead to a compromise between strong dimerization and solubility of the monomeric proteins.

However, much remains unclear about the oligomerization state and surface-adsorption process of proteins. We have therefore now used a combination of experiment and molecular-dynamics (MD) simulations to investigate the aggregation and surface adsorption of BLG in aqueous electrolyte solutions. The combination of experiment and MD simulations has proven extremely powerful, as the latter are in some cases the only tool that can help to understand complex macroscopic phenomena on the atomistic level.²¹

Furthermore, MD simulations allow direct insight into molecular structures that are sometimes inaccessible to experiment.^{21–23} In order to gain more insight into the behavior of β -lactoglobulin in different electrolytes, we have performed extensive molecular-dynamics simulations both at the atomistic and coarse-grained levels. To investigate the influence of sodium and potassium ions on the dimerization of BLG monomers, we also performed a thermodynamic-integration (TI)²⁴ study that in principle allows relative binding or complexation free energies to be calculated exactly.^{25–29} From a computational point of view, BLG poses a major challenge despite its stable, calyx-like structure: several studies report pH-dependent aggregation/oligo-/dimerization processes, and the actual association states remain controversial.^{30–32} Furthermore, it has been shown that BLG can form fibrillar or particulate gels that consist of larger aggregates such as amyloid fibrils or spherulites.^{33–35}

Also, it is unclear whether aggregation occurs in the bulk or at the interface. X-ray structural studies have revealed three possible protein–protein interfaces, called “dimer”, “lock-and-key”, and “loop interface”,³⁶ and pH-dependent transitions in chemical, physical, and spectroscopic properties that occur at around pH 7 (Tanford transitions).^{36,37} These transitions probably correspond to two possible loop conformations (loop EF, residues 85–90, see Figure S1 in the Supporting Information for a superimposition of structures), which themselves may be caused by two possible protonation states of Glu89 (anomalous $pK_a = 7.3$, H-bond with Ser116 if protonated).^{30,31,36–38} Figure 1 shows the positions of the three dimerization interfaces in the monomeric protein. Illustrations of the different dimers and the positions of the interfaces are provided in Figure S2 (Supporting Information).

MATERIALS, METHODS, AND COMPUTATIONAL DETAILS

Sum-Frequency Generation. Vibrational sum-frequency generation (SFG) is a powerful technique that can provide molecular-level information about molecular orientation and composition of electrified interfaces such as the protein-modified interfaces.^{1,41–43} In our broadband SFG spectrometer, a tunable (2–10 μm) femtosecond IR pulse with a bandwidth of $>200 \text{ cm}^{-1}$ is mixed with a picosecond pulse with a

wavelength of 800 nm and a bandwidth of $<6\text{ cm}^{-1}$. At the interface, a third wave with the sum-frequency of the two impinging light waves is generated which is then transferred to a spectrograph (Andor Shamrock 303i) and an ICCD camera (Andor iStar). All spectra were recorded with s-polarized visible, s-polarized sum frequency, and p-polarized IR-beams. In order to account for changes in pulse energy as a function of IR frequency, all spectra were normalized against the nonresonant SFG signal of an air plasma treated polycrystalline Au film. The SFG intensity can be written in the following form

$$I(\omega_{\text{SF}}) \propto |P_{\omega_{\text{SF}}}^{(2)}|^2 \propto |\chi^{(2)}|^2 = \left| \chi_{\text{NR}}^{(2)} + \sum_q \frac{A_q}{\omega_q - \omega + i\Gamma_q} \right|^2$$

with $A_q = N \int f(\Omega) \beta_q(\Omega) d\Omega$

(1)

Here the electric susceptibility is split into a nonresonant $\chi_{\text{NR}}^{(2)}$ contribution and one that is in resonance when the tunable IR pulse excites molecular vibrations at the interface. Since the oscillator strength A_q is an orientational average of the molecular hyperpolarizability, β_q with an angular distribution $f(\Omega)$, only molecules in noncentrosymmetric environments can contribute to the SFG intensity, while the phase of each vibrational mode q is determined by the net orientation of molecules. The latter leads to either constructive or destructive interferences between different vibrational modes or the nonresonant contribution. This can be used to determine molecular orientation or, in the simplest case if the absolute phase of a band is unknown, relative changes in molecule orientations. For air–water interfaces, SFG is inherently surface-specific, as molecules in the bulk are in a centrosymmetric environment and thus do not contribute to the SFG signal. At the interface, however, the prevailing bulk symmetry is broken and surface-adsorbed proteins and interfacial water molecules become SFG active.

Ellipsometry. The layer thickness of BLG layers was determined with a phase-modulated ellipsometer operating at a wavelength of 632.8 nm (Picometer Ellipsometer; Beaglehole Instruments; New Zealand). For each experiment, the sample solution was poured into a 10 cm diameter Petri dish and allowed to equilibrate for 30 min. Angle scans between 51 and 55° to the surface normal were performed with a step width of 0.5°. In order to ensure reproducibility, at least three measurements were recorded and averaged. Angle-resolved data from ellipsometry were fitted assuming a three-layer model with refractive indices of $n_{\text{water}} = 1.33$, $n_{\text{BLG}} = 1.40$, and $n_{\text{air}} = 1.00$ for the bulk solution, BLG layers, and air, respectively.

Sample Preparation. Details of the preparation of the 15 μM BLG solutions with a pH of 6.7 used in the SFG and ellipsometry experiments are provided in the Supporting Information. This concentration corresponds to one BLG monomer in an approximately 445³ Å³ box.

Computer Simulations. Monomer Simulations. As most computational approaches require fixed protein protonation states, we first used the H++,^{44–46} PROPKA,^{47–50} and Whatif⁵¹ pK_a-prediction tools to decide on the protonation states of BLGA. Several pH values of experimental interest were assessed. We focused on pH 6.2 for the monomer MD simulations to be consistent with initial experimental measurements. A consensus of the above tools, the literature, and initial experimental results showed that for pH 6.2 a BLG monomer, based on PDB^{52,53} code 3BLG,³⁶ with loop EF (residues 85–

90) closed (Glu44, Glu89, His146, and His161 protonated and designated “Glh44, Glh89, Hip146, Hip161” in the AMBER notation) is a reasonable starting structure for the MD simulations (total protein charge: −5 e). Furthermore, disulfide bridges between cysteines Cys66–Cys160 and Cys106–Cys119 were defined (“Cyx66–Cyx160, Cyx106–Cyx119”).

In order to study the distribution of the electrolyte ions around the protein in detail, atomistic MD simulations of a BLG monomer (PDB^{52,53} code 3BLG,³⁶ protonated as explained above for pH 6.2, represented by the Amber ff12SB force field)⁵⁴ in an octahedral box of 13 435 SPCE⁵⁵ water molecules were performed. Although the protein concentrations in our simulation cells are formally higher than in the experiment, the simulation methodology ensures that proteins in neighboring periodic cells do not interact, and thus, our simulations resemble diluted protein solutions. All atomistic MD simulations and many of the analyses were performed using Amber 12 and AmberTools 13.⁵⁴ Three independent sets of simulations were performed, each with an approximately 100 mM LiCl/NaCl/KCl electrolyte (5 M⁺ counterions plus 19 MCl, 99.5 mM Li⁺/Na⁺/K⁺). Ion concentrations of 100–150 mM correspond to physiological conditions, for which the biomolecular force field used was parametrized and validated. We therefore did not attempt to use higher salt concentrations in the MD simulations. Joung/Cheatham parameters were used for the ions.⁵⁶ In the simulations, the positions of the ions were randomized using Amber 12 ptraj⁵⁷ before starting the geometry optimizations (i.e., the positions of solvent and ions were swapped randomly). Langevin-dynamics simulations at 298 K and 1 bar were propagated over 600.5 ns for the systems containing Na⁺ and K⁺, and over 100.5 ns for the Li⁺ system. Detailed analyses of the ion distributions were performed in the 80.5–100.5 ns interval. More detailed information on the atomistic MD simulations and the analyses performed are provided in the Supporting Information.

Dimer Simulations. In order to investigate the possible influence of alkali-metal ions on the structure and stability of BLG dimers, we constructed three different dimers from the protein–protein contacts present in the X-ray structure 2BLG³⁶ (loop EF open), using the crystallographic information in the PDB structure file. These dimers are linked by the “dimer”, “loop”, and “lock-and-key” interfaces,³⁶ and we will name them accordingly. Views of these dimers and their contact surfaces are shown in Figures S2 and S4–S9 in the Supporting Information. Additionally, a dimer connected by the “loop” interface, based on 3BLG³⁶ (loop EF closed, Glh89 protonated), was simulated. This dimer is especially sensitive to the carboxylate–counterion–carboxylate bridging found previously for structurally persistent micelles.^{11,58,59} In the “dimer” and “lock-and-key interface” simulations, a simulation time of 61.5 ns was chosen and detailed analyses were carried out from 41.5 to 61.5 ns. In the case of the “loop interface” structure based on 2BLG (loop open), simulations were propagated until 209.5 ns and detailed analyses were performed for 101.5–209.5 ns. The simulation time was extended to 413.5 ns (analysis interval 101.5–413.5 ns) for the “loop interface” structure based on 3BLG (loop closed). More detailed information is provided in the Supporting Information.

Thermodynamic Integration. To obtain more robust information about the energetics of BLG dimerization, we calculated relative complexation free energies of sodium and potassium ions for the solvated protein (“bound”) and in water alone (“free”) according to the thermodynamic cycle shown in

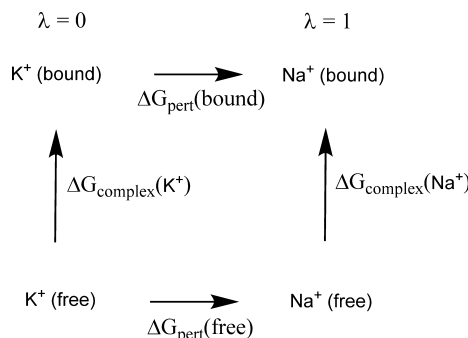


Figure 2. Thermodynamic cycle used in the free energy study

Figure 2. Perturbation free energies for the mutation of K⁺ into Na⁺ were computed using thermodynamic integration (TI) as implemented in Amber 12.^{54,60,61} Relative complexation free energies of a 100 mM K⁺ and a 100 mM Na⁺ electrolyte were calculated using eq 3. It is important to note that the system is in a dynamic equilibrium, where only a fraction of the M⁺ ions is coordinated to the protein while the rest is in solution, and not all potential complexation sites on the protein surface are occupied. Applying eq 3 yields the difference of the complexation free energies of a 100 mM Na⁺ and K⁺ electrolyte (with Cl⁻ counterions). The relative complexation free energy thus obtained reflects the difference between the system with protein and water present and the one with water only, but not the relative binding free energies of individual ions bonded to the protein. The calculations were performed both for a BLG monomer and for a dimer connected by the “loop interface”. More detailed information on the thermodynamic integration calculations is provided in the Supporting Information.

$$\Delta G_{\text{pert}}(\text{bound}) - \Delta G_{\text{complex}}(\text{Na}^+) - \Delta G_{\text{pert}}(\text{free}) + \Delta G_{\text{complex}}(\text{K}^+) = 0 \quad (2)$$

$$\begin{aligned} \Delta G_{\text{complex}}(\text{Na}^+) - \Delta G_{\text{complex}}(\text{K}^+) \\ = \Delta G_{\text{pert}}(\text{bound}) - \Delta G_{\text{pert}}(\text{free}) \end{aligned} \quad (3)$$

Coarse-Grained MD Simulations. In addition to the atomistic MD simulations in bulk solution, we performed a test simulation of a system consisting of a BLG monomer in a water slab in vacuum (vapor), which showed that the protein does not move much within the simulation time (71.5 ns) and that no surface adsorption is observed on this time scale. We therefore decided to use a coarse-graining (CG) approach,^{62–64} where on average four atoms are combined to form larger interaction sites. This approach not only reduces particle numbers in the simulation but also allows larger integration time steps (e.g., 30 fs) due to a smoother potential-energy surface. Thus, microsecond or even millisecond time scales are accessible for relatively large systems. To study the aggregation and surface-adsorption behavior of BLG, we performed three sets of CG simulations. First, a bulk system with evenly distributed BLG monomers was simulated. Additionally, two surface systems were set up. In one case, the protein monomers were distributed evenly in the aqueous phase in the starting structure, and in the other, they were initially placed near the surface. Each simulation was equilibrated for 333 ns, and data were subsequently collected during 5.1 μ s simulation.

In all three simulations, aggregates were formed quickly, and no clear surface preference was observed. As they did not lead

to new insight into the system, these coarse-grained MD simulations will only be discussed in the Supporting Information.

■ RESULTS

SFG Spectroscopy and Ellipsometry. In order to address the influence of LiCl, NaCl, and KCl salts on the adsorption of BLG and the interfacial water structure, we have studied different BLG adlayers with SFG and ellipsometry. Figure 3 shows vibrational SFG spectra in the region of C–H and O–H vibrational bands as a function of molar salt concentrations (the concentrations in the figure were selected to show the spectral changes in the frequency region of C–H stretching modes from aromatic residues ($\sim 3060\text{ cm}^{-1}$) in the best possible way). Very broad vibrational bands due to O–H stretching vibrations of tetrahedrally coordinated interfacial water molecules and molecules with lower coordination, respectively,^{65–67} can be inferred at 3200 and 3450 cm^{-1} . However, the very broad O–H feature indicates considerable dispersion of H-bonds, which causes inhomogeneous broadening of O–H stretching frequencies.

The depression in intensity around 3300 cm^{-1} , which has been suggested to originate from a coupling of the water bending overtone ($\nu = 0 \rightarrow \nu = 2$; $\sim 3300 \text{ cm}^{-1}$) with the O-H

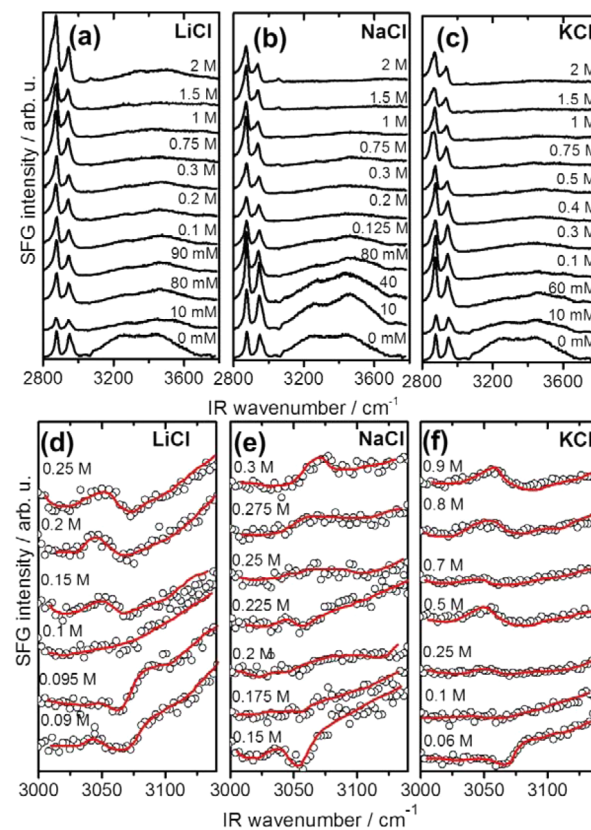


Figure 3. Vibrational SFG spectra of β -lactoglobulin (BLG) modified air–water interfaces in the region of C–H and O–H vibrational bands. Spectra were recorded for 15 μM BLG and different bulk concentrations of (a) LiCl, (b) NaCl, and (c) KCl. Concentrations were as indicated and were selected to show the spectral changes in the frequency region of C–H stretching modes from aromatic residues ($\sim 3060 \text{ cm}^{-1}$) in the best possible way. (d–f) Corresponding spectra where the $\sim 3060 \text{ cm}^{-1}$ band is shown in greater detail. Red lines guide the eye.

stretching mode,^{42,68} is just discernible. Additional strong vibrational bands are centered at 2877 and 2936 cm⁻¹ and a much weaker band at ~3060 cm⁻¹ (Figure 3). These bands originate from symmetric methyl (R—CH₃) stretching vibrations, a R—CH₃ Fermi resonance, and C—H stretching vibrations of aromatic residues of BLG at the air–water interface,^{1,41,69} respectively.

Figure 3 shows the change in overall intensity of the O—H bands as a function of LiCl, NaCl, and KCl concentrations. Increasing the salt concentration leads to a substantial decrease in O—H intensity and to a change in spectral shape of the 3060 cm⁻¹ band. In Figure 3d–f, we show the spectral region of the aromatic C—H stretching band in greater detail for concentrations at which the spectral changes occur. For LiCl, NaCl, and KCl salts and low ionic strengths, the C—H band overlaps with the O—H bands to generate a local minimum around 3070 cm⁻¹ that is followed by a less pronounced local maximum at ~3090 cm⁻¹. For concentrations >0.2 M, the apparent maximum is shifted to 3050 cm⁻¹ (Figure 3d–f). Although the change occurs for LiCl solutions at lower concentrations, the general trend of spectral changes is very similar for LiCl, NaCl, and KCl. For a further analysis of the SFG spectra, we recall the strong dependence of SFG vibrational bands on the molecular orientation of interfacial molecules, which comes from the coherent nature of the SFG process. Here, the amplitude of a SFG active vibrational band is not only a function of the number density of contributing molecules but also a function of the average molecular orientation at the interface (see eq 1). Since the intensity of C—H and O—H bands in Figure 3d–f does not change significantly for concentrations between 0.1 and 0.5 M, the observed changes in spectral shape probably indicate a change in the phase of either O—H or C—H bands. At low salt concentrations, the relative phases of O—H and aromatic C—H stretching bands cause destructive interference and result in a dip-like feature of the 3060 cm⁻¹ band, while, at high salt concentrations, interference leads to a local maximum at ~3060 cm⁻¹. In addition to the latter changes, the interference of O—H bands with the C—H bands (<3000 cm⁻¹) does also change, which can be best seen by a close inspection of the low frequency end (2800 cm⁻¹) of the SFG spectra in Figure 3a–c. Here, the SFG intensity decrease to nearly zero values at low salt concentrations, while at high concentrations (>0.3 M) the SFG intensities at 2800 cm⁻¹ are considerably higher. By fitting the spectra with model functions according to eq 1, we can show that the best description of the observed changes can be made by a change in C—H/O—H relative phase by $\pi/2$ that corresponds to a change in molecular orientation of 90°. A detailed discussion of possible molecular structure changes which are consistent with these observations can be found below and in the Supporting Information. At salt concentrations of 2 M, the intensities of O—H bands decrease to negligible values for NaCl and KCl solutions, while there is a weak but noticeable increase in O—H intensity when the LiCl concentration is increased from 1.5 to 2 M.

In order to corroborate the SFG experiments with a complementary method, we have investigated the thickness of BLG adsorption layers with ellipsometry (Figure 4). At salt concentrations <1 mM, the observed layer thickness of ~34 ± 2 Å is similar to the size of a monomer and consistent with previous neutron reflectivity measurements of BLG at air–water interfaces (37 ± 3 Å)^{70–72} but significantly less than the observed hydrodynamic diameter of 55 ± 4 Å^{70–73} of BLG in

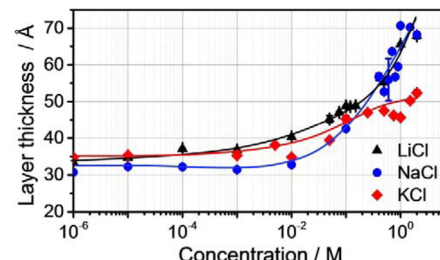


Figure 4. Layer thickness from ellipsometry as a function of LiCl, NaCl, and KCl concentrations. Lines are a guide to the eye.

solution. The thickness of the protein layer increases to 49, 45, and 43 Å for 0.1 M LiCl, KCl, and NaCl, respectively. A further increase in ionic strength leads to a thickness of ~69 Å for 2 M LiCl and NaCl, while for KCl a plateau at ~51 Å is found at high concentrations.

Monomer MD Simulations. Analysis of the atomistic MD simulations shows a clear accumulation of Li⁺, Na⁺, and K⁺ near the carboxylate oxygens of Asp and Glu (formation of contact ion pairs, CIP), and to a much lesser extent near the backbone carbonyl oxygen atoms. This accumulation decreases with increasing size of the alkali-metal ion (Li⁺ ≫ Na⁺ > K⁺). Li⁺ is also found to bridge strongly between neighboring carboxylate groups to form ion triplets. A detailed analysis of cation accumulation near carboxylic moieties, ordered according to the number of ion contacts in the first solvation shell of the carboxylic oxygen atoms of individual Asp/Glu residues, is shown in Figure 5. It is especially noteworthy that the order of

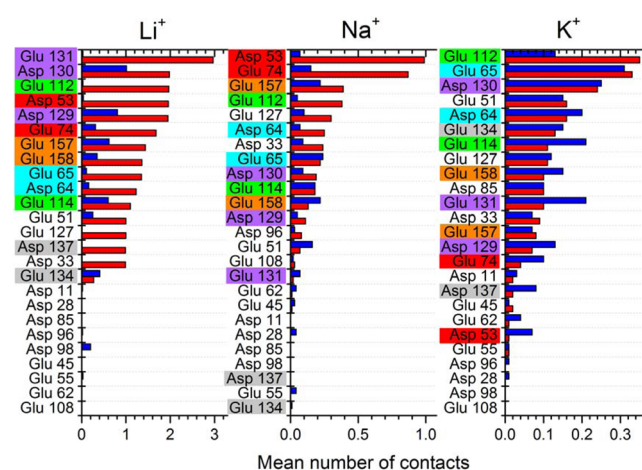


Figure 5. Mean numbers of contacts between alkali-metal cations and the carboxylic oxygens of individual aspartate and glutamate residues (red bars, first coordination shell; blue bars, second coordination shell) for solutions of the BLG monomer in 100 mM Li⁺, Na⁺, and K⁺ salts. The density of the metal ions decreases on going down the columns (ordering according to the number of contacts in the first coordination shell). Boxes of the same color indicate residues that are geometrically close to each other and are therefore able to coordinate the same metal cation to form ion triplets or multiplets. Because of the definition of the search mask used in the analysis, metal ions coordinated to two or more carboxylates are counted once in each interaction. Thus, the contact numbers in this figure can only be considered as a measure for the ranking; their sums are not equal to the contact numbers in Table 1, where the contact numbers calculated for all Asp/Glu carboxylates in the system are reported, which are unaffected by a bi/multiple coordination of the metal.

the enrichment of metal cations around specific carboxylic groups differs according to the metal cation and the type of carboxylic group (Asp or Glu) to which it is bonded. Chloride anions are not enriched significantly near positively charged residues (Lys, Arg).

The distributions of the cations are shown in Figure 6, and a complete analysis is given in Table 1. The distribution of Li^+ , Na^+ , and K^+ together with Cl^- ions is shown in Figure S12 (Supporting Information). The mean numbers of contacts and the residence times calculated for Li^+ , Na^+ , and K^+ in the first and second coordination shells around all Asp/Glu carboxylate and backbone oxygen atoms in the system vary significantly between the three metals. The former show a significant overcompensation of the charge when 100 mM Li^+ is coordinated to the protein carboxylates and backbone oxygens (the net charge of protein with the first and second Li^+ shells is +10.4), and almost exact charge compensation for 100 mM Na^+ (net charge +0.3e) and 100 mM K^+ (net charge -0.7e). Although the difference between Na^+ and K^+ is not very large, the experimental trend is reproduced correctly. If Cl^- binding to positively charged residues (Lys, Arg) is considered in the estimation of the total charge, net charges of 9.0, -0.6, and -1.3e are obtained. The relatively small effect of considering Cl^- reflects the fact that the force field employed does not show a significant enrichment of anions near the positively charged residues Lys and Arg. The radii used to count the numbers of ions in the first and second coordination shells were determined from the RDFs of the ions around a particular moiety (Table S1, Supporting Information). RDF plots of M^+ around Asp/Glu carboxylic oxygens and of Cl^- around Lys ammonium and Arg guanidinium nitrogens are shown in Figures S10 and S11 (Supporting Information). These RDF plots also show that Cl^- is not significantly enriched near positively charged residues. Interestingly, the net charges calculated for the protein with all M^+ and Cl^- ions within 6.4 Å of any protein heavy (non-hydrogen) atom are very close to the values given above (+8.8, -0.5, and -1.0e), which indicates that ion coordination to carboxylates, backbone oxygens, and, to a much lesser extent, Lys and Arg side chains dominates the ion adsorption to the protein. Figure 7 shows the total charge of the protein and the surrounding ions as a function of the distance from the protein center of mass, calculated from the protein net charge (-5 e at pH 6.2) and the integrals of the RDF bin values of the cations and the anions. At distances greater than the approximate radius of the protein (radius of gyration approximately 15 Å, see below), first metal cations are coordinated in the order $\text{Li}^+ > \text{Na}^+ > \text{K}^+$, and then the Cl^- cloud compensates the total charge until the total charge of the system (electrically neutral) is reached. It should, however, be noted that BLG is not a spherical particle.

The residence times of the cations coordinated to carboxylates at 100 mM decrease in the order Li^+ (mean = 11.5 ns), Na^+ (370 ps), and K^+ (30 ps). However, individual sodium ions can assume bridging positions between carboxylates for times up to 15 ns, compared to 20 ns for Li^+ and only 1.3 ns for K^+ . These results are consistent with previous work, which showed much more prevalent Na^+ :carboxylate CIPs relative to K^+ for polyanionic micelles.^{11,58,59} This metal–ion coordination to carboxylates with protein charge compensation or overcharging is consistent with the results of SFG measurements (see discussion below). Overall, we observe a complex balance of several equilibria, e.g., M^+ –carboxylate, M^+ –backbone-carbonyl, and M^+ –water coordination. While

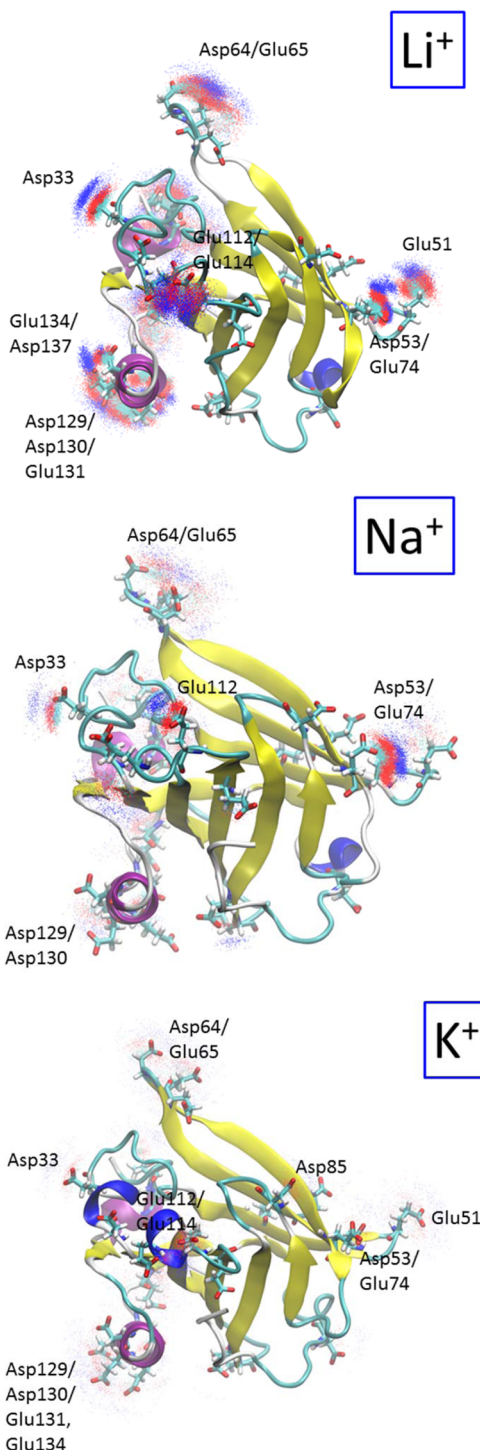


Figure 6. Li^+ (blue, top), Na^+ (blue, middle), and K^+ (blue, below) distribution around Asp and Glu carboxylates (oxygen atoms, red; carbons, cyan) of a BLGA monomer. Only contact ion pairs are shown; other ions (M^+ further away than first solvation shell and Cl^-) and water were omitted for clarity. Simulations with 100 mM $\text{LiCl}/\text{NaCl}/\text{KCl}$, analysis interval 80.5–100.5 ns, all frames fitted on minimized structure, only every 10th frame for $\text{Li}^+/\text{Na}^+/\text{K}^+$ CIP, and carboxylate oxygens/carbons shown for clarity. Figures were created using a custom-made script^{11,58,59} and VMD.⁷⁴

we find the expected order for the mean numbers of the ion contacts in the first coordination shell of the carboxylate oxygens, this number has a maximum for coordination to Na^+ if the coordination to the backbone carbonyl oxygens is assessed

Table 1. Contacts and Residence Times (ps) of Ions and Water in the First and Second Coordination Shells around Carboxylate Oxygens of Asp/Glu, Backbone Carbonyl Oxygens, Ammonium/Guanidinium Nitrogens of Lys/Arg and within 6.4 Å of Any Heavy (Non-Hydrogen) Atom of the BLG Monomer in Different Salt Solutions (Analysis Interval: 80.5–100.5 ns)^a

		100 mM LiCl	100 mM NaCl	100 mM KCl		100 mM LiCl	100 mM NaCl	100 mM KCl
M^+/COO^-								
mean number of contacts	shell 1	15.0	3.48	2.06	maximum residence time	285	1761	581
	shell 2	0.20	1.19	1.59	Water Oxygen/Backbone Oxygen			
mean number of contacts per residue	shell 1	0.60	0.14	0.08	mean number of contacts	shell 1	116.0	115.8
	shell 2	0.01	0.05	0.06	shell 2	318.8	324.8	323.9
mean residence time	shell 1	11 543	370.0	30.0	mean number of contacts per residue	shell 1	0.72	0.72
	shell 2	8.3	19.5	8.0	shell 2	1.98	2.02	2.01
maximum residence time	shell 1	20 000	15 350	912	Cl ⁻ /Lys-N			
	shell 2	462	594	122	mean number of contacts	shell 1	0.25	0.18
Water Oxygen/COO ⁻								
mean number of contacts	shell 1	105.8	116.6	119.2	shell 2	1.08	0.75	0.49
	shell 2	206.9	281.4	291.7	mean number of contacts	0.06	0.01	0.02
mean number of contacts per residue	shell 1	4.23	4.66	4.77	Cl ⁻ /Arg-N ($\leq 6.4 \text{ \AA}$)			
	shell 2	8.28	11.26	11.67	mean number of contacts	16.29	5.92	4.99
mean residence time	shell 1	9.8	13.4	15.5	mean number of contacts	2.52	1.41	1.01
	shell 2	4.1	5.6	5.9	Cl ⁻ /Heavy Atoms ($\leq 6.4 \text{ \AA}$)			
maximum residence time	shell 1	2663	1768	6593	mean number of contacts			
	shell 2	545	1365	3754	mean number of contacts			
$M^+/Backbone\ Oxygen\ (First\ Shell)$								
mean number of contacts		0.16	0.65	0.61	mean number of contacts			
mean residence time		16.4	60.8	24.5	mean number of contacts			

^aContacts per residue were obtained by dividing the total number of coordinated ions by the number of deprotonated Asp and Glu carboxylates (25) and backbone carbonyl oxygens (161 without C-terminus).

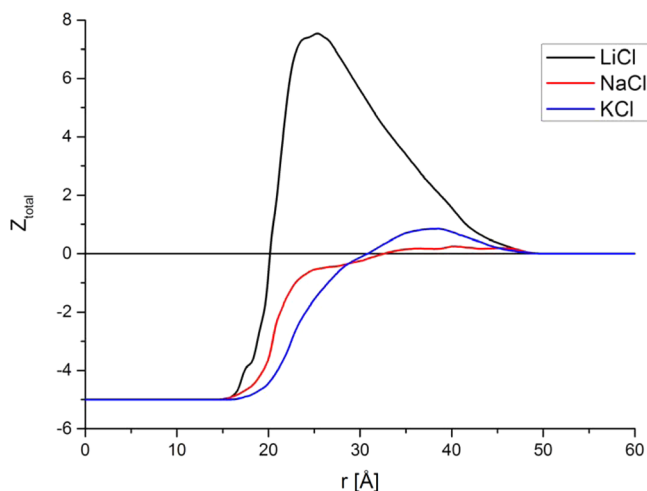


Figure 7. Total charge of the protein and the surrounding ions as a function of the distance from the protein center of mass, calculated from the protein net charge (-5 e at pH 6.2) and the integrals of the RDF bin values of the cations and the anions: $Z_{\text{total}} = Z_{\text{protein}} + Z_{\text{cations}} - Z_{\text{anions}}$. For details, see the Supporting Information.

(Table 1). In the case of lithium, on average, 15 of the 24 Li^+ ions present in the system are bound to the carboxylates and are thus not available for backbone oxygen coordination.

While the absolute numbers presented in Figure 5 and Table 1 might be improved by performing more extensive sampling, and might also be force-field-dependent, we believe that the qualitative trends are reproduced correctly. Figure 5 shows that the three cation types experience quite different affinities to carboxylates, and additionally gives a finer analysis of binding to individual carboxylic moieties, depending on the type and local environment of a particular amino acid. This quantitative analysis is subject to sampling errors and that the results should be taken in this light.

The strong overcharging by Li^+ could in principle lead to a destabilization of the BLG dimer. However, in the ellipsometry experiments, such a dissociation was not observed. This shows that local, specific interactions dominate and need to be analyzed in detail and that net-charge effects alone cannot be used to explain protein aggregation in systems like BLG.

The enrichment of M^+ cations near carboxylic moieties also means that carboxylate-rich surface patches of the protein (i.e., hydrophilic patches) can become potential dimerization surfaces in the presence of lithium or sodium ions.

In addition to the above analyses, we also calculated the radii of gyration of the monomers in 100 mM LiCl (14.9 Å), NaCl (14.9 Å), and KCl (14.8 Å, Figure S14, Supporting Information). These are similar for the three electrolytes and agree well with the thickness of a BLG monolayer at the air–water interface as determined by ellipsometry (~34 Å).

Dimer Simulations. In order to identify dimers whose structure is influenced by the presence of NaCl or KCl electrolytes, we simulated the “loop”, “dimer”, and “lock-and-key interface” structures of the dimers, as outlined in the Materials, Methods, and Computational Details section. Simulations were performed in both 100 mM NaCl and KCl solutions. These dimers were simulated with loop EF (residues 85–90) “open” (corresponding to an approximate pH > 7, structure based on PDB^{52,53} structure 2BLG),³⁶ and additionally, the “loop interface dimer” was simulated with loop EF “closed” (approximately pH < 7, based on 3BLG,³⁶ Glh89 in both monomers protonated, hydrogen bond between atoms Oe2 of Glh89 and O of Ser116 in both monomers). The root-mean-square deviation (RMSD), calculated for all C_α atoms after fitting each structure on the minimized X-ray structure, the radius of gyration, calculated for all atoms, and the distance of the centers of mass of all C_α atoms in monomers 1 and 2 were used as measures of geometry change in the simulations. These are shown in Figures S17–S19 and S22–S24 (Supporting Information) for the “loop interface dimers” and in Figures S28–S30 and S33–S35 for the “dimer” and “lock-and-key” interface dimers. The dimer structures connected by the “loop interface” are shown in Figures S15, S16, S20, and S21 (Supporting Information); the corresponding figures for the structures bridged by the “dimer” and “lock-and-key” interfaces are shown in Figures S26, S27, S31, and S32 (Supporting Information).

Visual inspection of the simulated structures and analysis of the C_α atom RMSD, the radius of gyration, and the distance between the centers of mass of all C_α atoms in monomers 1 and 2 (Figures S26–S35, Supporting Information) show that the “dimer” and “lock-and-key” interface structures do not undergo significant geometry change during simulation. Therefore, these simulations were terminated after 61.5 ns and we conclude that these dimers can exist in the experimental system but are not sensitive to exchange of the alkali ions (Na⁺, K⁺) in the electrolyte (i.e., the distribution of carboxylates on the dimerization surfaces is not ideal for the formation of bridging interactions by metal cations for these dimers).

In contrast, dimers connected via the hydrophilic “loop interface” are sensitive to the kind of alkali ions (sodium, potassium) in the solution. Figures S15 and S20 (Supporting Information) show that sodium cations are significantly enriched in regions that bear carboxylic amino acids (glutamate, aspartate), especially in the interfacial region between the monomers. This observation has been confirmed in the thermodynamic integration calculations (see below). Analyses of the C_α atom RMSD, the radius of gyration, and the distance between the centers of mass of all C_α atoms in monomers 1 and 2 (Figures S17–S19 and S22–S24, Supporting Information) show that both the presence of Na⁺ and K⁺ affects the geometry of the dimer compared to the starting structure (the minimized dimers constructed from the X-ray structure), and that Na⁺ is inserted more frequently between Asp and Glu carboxylate groups than K⁺ and thus disrupts the native interaction between the protein monomers, which is dominated by interactions of lysine ammonium groups (and the Asn63 amide moiety) with aspartate and glutamate carboxylates. In our simulation of the “loop interface” dimer with loop EF closed (based on PDB code 3BLG), we observe that the dimer bridged by carboxylate–sodium–carboxylate interactions is stable throughout the entire simulation time (413.5 ns, see Figure S20, Supporting Information), while in the simulation with

potassium the dimer dissociates after 246 ns and the monomers remain separated for 61 ns. After rotating relative to each other, the monomers form a new contact from 307 ns on, which is stable until the end of the simulation (413.5 ns). This new dimer is connected by lysine–carboxylate interactions between Lys77–Glu158, Lys75–Glu65, Asp11–Lys70, Lys14–Glu55, and Lys8–Glu44 in the two monomers. The latter interaction of Lys8 and Glu44 is typical for the “lock-and-key interface”, and we identified the newly formed dimer to be structurally related to the corresponding dimer but with one of the monomers rotated by approximately 90°. These changes are well reflected in the analyses of the C_α atom RMSDs, the radii of gyration, and the distances between the centers of mass of all C_α atoms of the monomers (Figures S22–S24, Supporting Information). We note that the geometry changes described here are most probably not yet converged and much longer simulations or more sophisticated, accelerated techniques are required to find geometries close to the free energy minimum.

If loop EF is in an open conformation (at pH values \geq 7–8, PDB structure 2BLG), it acts as an additional anchor between the monomers. Thus, (partial) insertion of ions has a smaller effect on monomer separation, which is illustrated by the virtually identical mean distances of the centers of mass of the C_α atoms in the two monomers (calculated for the time interval 101.5–209.5 ns): 31.5 Å for Na⁺ and 31.4 Å for K⁺ (Figure S19, Supporting Information), compared to 33.8 Å in the simulation with Na⁺ and loop closed (3BLG) and 33.2 Å in the corresponding simulation with K⁺ (Figure S24, Supporting Information, mean values for the same time interval). For this time interval (101.5–209.5 ns, prior to dissociation in the K⁺ simulation with closed loop), the difference in C_α atom RMSDs between the Na⁺ and K⁺ simulations is more pronounced in the simulation with loop EF open (2BLG, 9.5 Å for Na⁺ and 5.7 Å for K⁺, Figure S17, Supporting Information) than in the one in which loop EF is closed (3BLG, 9.2 Å for Na⁺ and 7.6 Å for K⁺, Figure S22, Supporting Information). This indicates that, in the case of the simulation with loop EF closed (3BLG), the effects of Na⁺ and K⁺ on the dimer structure during the first 209.5 ns are more similar than in the simulation with loop EF open (2BLG). This is because in the latter case Na⁺ ions can be inserted more easily between the monomers, which are connected more strongly by their open EF loops, than K⁺ ions. The effect that Na⁺ ions are capable of bridging carboxylates more strongly than K⁺ ions has been observed previously.^{11,58,59}

Figure S25 (Supporting Information) shows that loop EF stays closed over most of the simulation time in the simulations in which it starts closed (3BLG). The closed conformation is stabilized by a hydrogen bond between atoms Oe2 of Glh89 and O of Ser116 in both monomers.

The radii of gyration for the dimers are about 22 Å for the “loop interface” dimers (21.9, 21.8, 22.6, and 22.4 Å, Figures S18 and S23, Supporting Information), and also for the “dimer” (21.9 and 21.9 Å, Figure S29, Supporting Information) and the “lock-and-key” interface structures (21.7 and 21.9 Å, Figure S34, Supporting Information). These values agree well with the thicknesses of protein layers at a salt concentration of 0.1 M, as determined by ellipsometry (approximately 46 Å (49 Å for 0.1 M LiCl, 45 Å for 0.1 M KCl, and 43 Å for 0.1 M NaCl), see above).

Thermodynamic Integration. Standard MD analyses and analyses of the free energy gradients with respect to the coupling parameter λ (used for integration) were performed for

$\lambda = 0.1$ ("K⁺-like") and $\lambda = 0.9$ ("Na⁺-like"). Plots of the gradients are shown in Figures S36, S37, S40, S43, and S48 (Supporting Information). All gradients were sufficiently stable after equilibration. Plots of the ensemble averages of $\langle dV/d\lambda \rangle$ vs λ yielded smooth curves, which can be integrated easily (Figures S38, S41, and S49 in the Supporting Information).

The integrated perturbation free energies are listed in Tables S2–S6 (Supporting Information) and are plotted versus simulation time in Figures S39, S42, and S50 (Supporting Information). Standard deviations and standard errors were obtained from batch averaging. They are generally smaller in the "free" simulation legs, i.e., when only ions and water are present (standard errors 0.02 and 0.04 kcal mol⁻¹ for the systems containing as many ions and water as in the monomer and dimer simulations, respectively), than in the "bound" case (ions, water, and protein, standard errors 0.05–0.08 and 0.14 kcal mol⁻¹). These are acceptable measures of the numerical precision of the simulations, as shown previously.²⁸ Inspection of the plots of the integrated free energies shows that the systems are sufficiently equilibrated after about 5 ns, with the exception of the monomer simulation with an alternative protonation state (Glh131 protonated instead of Glh74), where a longer equilibration (and, hence, extended simulation in general) was required (15.5 ns). Of particular interest are the differences of the "bound" and "free" perturbation free energies, which describe the relative complexation free energies of sodium and potassium ions, in the system with protein and water ("bound") and in water only ("free"), according to eq 3 and Figure 2. These are summarized in Table 2, which shows

Table 2. Relative Complexation Free Energies of Sodium and Potassium Ions, in the System with Protein and Water ("Bound") and in Water Only ("Free"), according to eq 3^a

system	time (ns)	$\Delta G_{\text{complex}}(\text{Na}^+) - \Delta G_{\text{complex}}(\text{K}^+)$	SD	SE
monomer (Glh74)	5.5–25.5	−0.50	0.26	0.08
monomer (Glh131)	15.5–35.5	−1.00	0.17	0.05
dimer	5.0–25.0	−2.91	0.95	0.15

^aAll energies are given in kcal mol⁻¹. Standard deviations (SD) and standard errors (SE) were obtained by Gaussian error propagation. For the monomer, two different protonation states were examined (see the Materials, Methods, and Computational Details section).

that the complexation free energy of Na⁺ is generally more negative than that of K⁺, as expected. However, these numbers differ for the three cases investigated: A relative complexation free energy of −0.5 kcal mol⁻¹ was found for the monomer in which Glh74 was protonated. In this protonation state, Glh74 is not available to coordinate a metal cation together with Asp53 (which would result in the formation of an ion triplet). It is also positioned unfavorably on the contact surface ("loop interface") on which the ion triplets most often form. If Glu74 is left deprotonated and Glh131 (which is far from the dimerization interface and has been shown not to be involved significantly in the formation of ion triplets for Na⁺ and K⁺, see Figure 5) is protonated instead, the value of $\Delta\Delta G$ changes to −1.00 kcal mol⁻¹. This demonstrates the effect of the formation of an ion triplet together with Asp53 nicely. This common coordination of a metal cation by Glu74 and Asp53 is more pronounced for Na⁺ than for K⁺ (see Figure 5). A $\Delta\Delta G$ value of −2.91 kcal mol⁻¹ was found for the dimer system. This much more

negative value emphasizes the importance of bridging by sodium compared to potassium in dimer formation. In particular, bridging interactions between the carboxylates of Glu74 and Asp53 in the first monomer and between Asp85 in the first monomer and the backbone carbonyl oxygen and the carboxylate of Glu62 in the second are important (formation of ion triplets and multiplets, see Figure 8 and Figure S51,

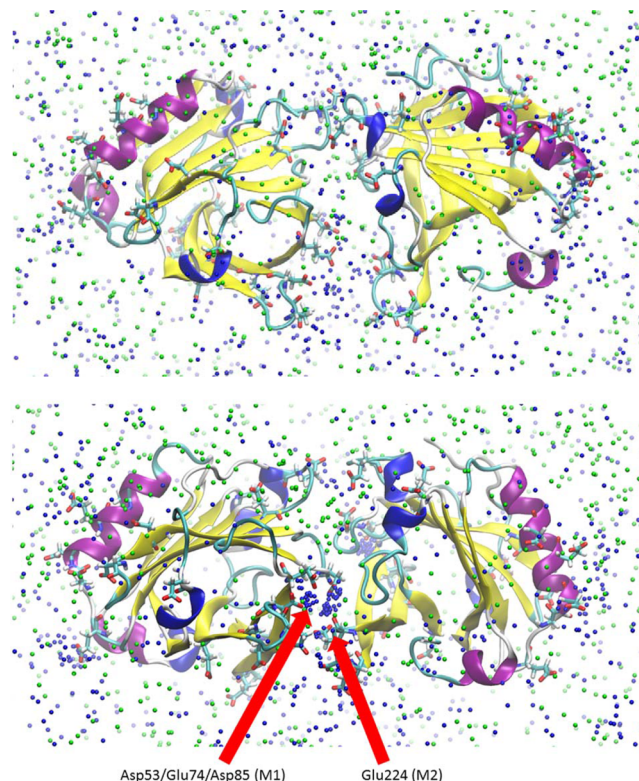


Figure 8. Thermodynamic integration: structure of dimer after 25 ns (cartoon representation, Asp and Glu as sticks). Every 50th structure of MCl in the time interval 5.0–25.0 ns shown. M⁺, blue; Cl[−], green. Above, $\lambda = 0.1$ ("K⁺-like"); below, $\lambda = 0.9$ ("Na⁺-like"). Figures were created using VMD.⁷⁴

Supporting Information, for an illustration). Interestingly, Asp85 itself is not found to be strongly coordinated by Na⁺ or K⁺ in the monomer simulations (see Figure 5). Thus, the presence of a second monomer changes the ion-distribution pattern on the protein surface significantly. Another ion triplet is observed between Asp53 and Glu74 in the second monomer, but this one is not involved in the bridging between the monomers. The influence of the relative complexation free energies on the dimerization free energy of two BLG monomers can be assessed by subtracting twice the monomer value from $\Delta\Delta G_{\text{complex}}$ obtained for the dimer. Thus, values of −1.91 and −0.91 kcal mol⁻¹ are obtained for the simulations with Glh74 with Glh131 protonated, respectively. Thus, sodium counterions favor dimerization in both cases compared to potassium. This situation is analogous to that found for polycarboxylate micelles.¹¹

DISCUSSION

We have investigated the influence of counterions and salt concentrations on the aggregation behavior and the surface adsorption of β -lactoglobulin in water. SFG and ellipsometry experiments have provided insight into the situation at the air–

water interface. However, initial atomistic and coarse-grained (CG) simulations did not show protein surface adsorption on the time scales studied (70 ns and 5.4 μ s, respectively). This may either mean that surface aggregation takes place slower than on the microsecond time scale or that the coarse-grain model is unable to reproduce the effects expected. We have therefore resorted to atomistic models of protein monomers and dimers in bulk solution in order to study the influence of different salt solutions.

SFG and ellipsometry indicate substantial changes in the interfacial structure of BLG-modified air–water interfaces as a function of salt concentration. The decrease in O–H intensity with ionic strength can be attributed to a change in the strength of the interfacial electric field (see the Supporting Information) caused by charge screening and possibly by ion specific effects such as the complexation of alkali ions with carboxylate groups on the protein surface, as observed in the MD simulations. These indicate a preference for Li⁺ and Na⁺ over K⁺ when binding to carboxylates, which has also been observed for proteins and model peptides in previous studies, e.g., by Jungwirth and co-workers,^{3,75–79} by Cremer and co-workers,⁸⁰ and by ourselves for polyanionic micelles.^{11,58,59} This order is even maintained if solvent-shared ion pairs, rather than contact ion pairs, are formed preferably.⁸¹ Chloride anions are not significantly enriched near positively charged residues (Lys, Arg), as also found by Jungwirth and co-workers.^{82–84} While these findings are *per se* not new, the system used in our study offers an opportunity to investigate ion effects on different mechanisms of protein dimerization. The thermodynamic integration part of our study is, to our knowledge, the first application of this kind to study electrolyte effects on protein dimerization.

Changes in SFG intensity are accompanied by a change in spectral shape and an increase in thickness of the BLG surface layer that occurs at similar ionic strength. We relate this to changes in net orientation of either interfacial water or BLG molecules (for a detailed discussion, see the Supporting Information). The observed layer thickness at low ionic strengths is consistent with the size of monomeric BLG molecules (radii of gyration as obtained from the monomer MD simulations approximately 15 Å, see the Results section). There is good agreement between the layer thickness measured at 0.1 M salt concentrations and the hydrodynamic diameter of BLG dimers from our MD simulations (radii of gyration approximately 22 Å, see the Results section). We therefore propose that the change in the relative phase of C–H and O–H bands and the increase in layer thickness points to a transition from a protein adsorbate layer with densely packed monomers to a BLG bilayer. The latter is possibly dominated by BLG dimers with their long axis parallel to the surface normal. Our observation that monomers and dimers prevail at the pH used in this study is consistent with the literature.^{70–73}

The observed changes in SFG vibrational spectra are more pronounced for LiCl than for NaCl and KCl, which is consistent with the MD simulations of BLG proteins in bulk solution. Here, ion pairing between alkali-metal cations and carboxylate anions at the protein surface can stabilize BLG dimers. The ion-pair and ion-multiplet formation indicated by the MD simulations necessarily leads to changes of the BLG net charge. Since the probability of the formation of ion pairs or triplets with Asp or Glu carboxylates (Figure 5) increases in the order K⁺ < Na⁺ < Li⁺, it is not surprising that the decrease in O–H intensity and the relative change in phase with an

increase in salt concentration is more pronounced for LiCl. In fact, we only observe first a dramatic decrease in O–H intensity that is followed by a weak but noticeable recovery of the O–H intensity at 2 M LiCl concentration (Figure 3a). This increase in intensity could be related to charge reversal and subsequent overcharging of BLG due to the comparatively high propensity of Li⁺ to form ion–ion complexes at the BLG surface, as observed in the molecular dynamics simulations (see the Results section). These findings are in good agreement with previous work by Jungwirth and co-workers, who studied charge compensation and overcharging of tetra-aspartate by coordination with mono-, bi-, and trivalent cations.⁷⁶

Aggregation and surface adsorption of β -lactoglobulin is a complex phenomenon that depends on several variables. Solution pH determines the specific protonation pattern on the protein surface, which itself has a pronounced effect on protein–protein interaction in the absence of bridging metal cations, e.g., by interacting Lys-ammonium groups and Asp/Glu-carboxylates. Due to the requirements of the MD methodology, this protonation pattern was kept fixed in the current study. Future studies might involve constant pH MD simulations^{85,86} that alter the protonation pattern dynamically or thermodynamic integration between protonation states that allows a more realistic assignment of protonation states. A major influence of pH on BLG dimerization is given by the pH dependent conformation of loop EF, which is commonly reported to be open for pH values >7 and closed for pH < 7. These two conformations were treated as independent simulations in the present study, and it was found that the loop conformation does indeed have an influence on the “loop interface” dimer, as it acts as an additional anchor between the monomers.

Metal coordination of carboxylates allows a bridging interaction between Asp/Glu residues, both within one monomer and between two monomers. The MD simulations of different dimers have shown that only the “loop interface” dimer is sensitive to the kind of ions present in solution so that we conclude that only this dimer is determined by bridging metal coordination. Our thermodynamic integration study confirms the thermodynamic effect of the increased ability of Na⁺ to bridge between carboxylates and, hence, between monomers compared to K⁺.

The MD simulations indicate that, in addition to net charge effects of the whole protein, the local complexation of individual carboxylates contributes to the effects seen in SFG spectroscopy. This probably occurs by changing the binding geometries of coordinated water molecules and thus reversing the local electric field that acts on a given water molecule when a coordinating COO[−] is replaced by M⁺ (see Figure S13, Supporting Information, for an illustration). Thus, we can now enhance the simple concept of charge compensation/overcharging by a more detailed atomistic picture.

Generally, hydrophobic patches are frequently found to be important for protein dimerization. However, the surface amino-acid pattern of BLG means that this effect only plays a major role for the dimer connected by the “dimer interface”, where β -strands of the two monomers interact with each other (“cross-beta interaction”), and, additionally, an area of higher hydrophobicity is found in the contact surface (Figures S6 and S7, Supporting Information). Additionally, one of the protein surface patches involved in the formation of the “lock-and-key” interface shows a slightly enhanced hydrophobicity (Figures S4 and S5, Supporting Information).

White and co-workers used X-ray and neutron reflectometry to study BLG at the air–water interface, both with and without denaturant.⁷⁰ For the system without denaturant, they observed monomer adsorption. They argued that the protein surface that forms the interface for dimerization is largely hydrophobic, and we assign this surface to be the one involved in the formation of the “dimer interface”. Therefore, it is likely that the monomer adsorbs preferentially to the air–water interface with this more hydrophobic patch toward the interface.⁷⁰ Figure S53 (Supporting Information) shows four monomers of BLG as they are oriented in the crystal, and the possible protein–protein interfaces relative to each other. We can speculate that, if the more hydrophobic “dimer interface” is preferentially located at the air–water interface, the contacts in the first BLG monolayer are determined by the “loop interface” and the “lock-and-key interface”, whereas a second layer of BLG monomers can be bridged with the first one via “dimer interfaces”.

CONCLUSIONS AND OUTLOOK

We have begun constructing a detailed atomic model of protein aggregation that goes further than simple pictures such as the aggregation via hydrophobic patches or the dominant influence of the effective total charge of the protein monomers. Adsorption at the air–water interface could not be reproduced in preliminary atomistic and coarse-grain simulations, so that we have concentrated on protein aggregation in bulk solution. The results of these simulations are consistent with both SFG and ellipsometry experiments.

Our work also suggests either that the coarse-grained model employed cannot reproduce the surface aggregation process of BLG or that the time scale of this process exceeds that of the 5 μ s simulation reported here. Future studies of the fine structure of water, electrolyte, and large protein aggregates at the air–water interface will thus require very long simulations and/or atomistic force fields, despite the higher computational effort. Furthermore, our method of postprocessing classical MD ensembles with all-QM⁸⁷ or QM/MM techniques^{21,23} can be used to calculate hyperpolarizabilities,^{88,89} which will allow a direct comparison with experimental results from second-order spectroscopy.

The present study shows that molecular simulations can most valuably complement experimental studies, as they allow a direct view on an atomistic scale, which is in many cases inaccessible by experiments.

ASSOCIATED CONTENT

Supporting Information

Additional figures and tables showing (a) illustrations of monomer conformations and the different dimers investigated, (b) sample preparation for SFG spectroscopy and ellipsometry, (c) detailed discussion of the SFG spectra, (d) detailed views of the different dimers investigated in the MD study, (e) computational details of monomer, dimer, and thermodynamic integration simulations, (f) minima in the radial distribution functions used to define first and second coordination shells (monomer simulations), (g) radial distribution functions of M⁺ around Asp and Glu carboxylate oxygens (monomer simulations), (h) radial distribution functions of Cl⁻ around Lys ammonium and Arg guanidinium nitrogens (monomer simulations), (i) illustrations of the ion distributions in the monomer simulations, (j) view of the water environment around a carboxylate pair with and without coordinated cation,

(k) radii of gyration as obtained from monomer simulations, (l) illustrations of the ion distributions and the structures in the dimer simulations, (m) RMSDs, radii of gyration, and distances as obtained from the dimer simulations, (n) gradients and integrated perturbation free energies as obtained from the thermodynamic integration calculations (salt solution without protein and with monomer or dimer), (o) RMSDs, radii of gyration, and distances as obtained from the thermodynamic integration simulation of the dimer, (p) protein diffusion coefficients, (q) details and results of the coarse-grained simulations, and (r) hypothetical arrangement of BLG monomers at the air–water interface. This material is available free of charge via the Internet at <http://pubs.acs.org>.

AUTHOR INFORMATION

Corresponding Author

*Phone: +49 9131 85 22948. Fax: +49 9131 85 26565. E-mail: Tim.Clark@fau.de.

Notes

The authors declare no competing financial interest.

ACKNOWLEDGMENTS

This work was supported by the Deutsche Forschungsgemeinschaft as part of the Excellence Cluster *Engineering of Advanced Materials* and through the Leibniz program and the DFG-AiF cluster project on “Protein Foams” (PE427/21-1). We thank the Regionales Rechenzentrum Erlangen for computing facilities. We also wish to thank Christof Jäger for analysis scripts from his previous work (ion residence times).^{11,58,59} We would like to thank Ulrich Kulozik (Technische Universität München, Germany) and his group for supplying us with high-quality β -lactoglobulin.

REFERENCES

- Chen, X.; Flores, S. C.; Lim, S.-M.; Zhang, Y.; Yang, T.; Kherb, J.; Cremer, P. S. Specific Anion Effects on Water Structure Adjacent to Protein Monolayers. *Langmuir* **2010**, *26* (21), 16447–16454.
- Lund, M.; Vrbka, L.; Jungwirth, P. Specific Ion Binding to Nonpolar Surface Patches of Proteins. *J. Am. Chem. Soc.* **2008**, *130* (35), 11582–11583.
- Heyda, J.; Pokorna, J.; Vrbka, L.; Vacha, R.; Jagoda-Cwiklik, B.; Konvalinka, J.; Jungwirth, P.; Vondrasek, J. Ion Specific Effects of Sodium and Potassium on the Catalytic Activity of Hiv-1 Protease. *Phys. Chem. Chem. Phys.* **2009**, *11* (35), 7599–7604.
- Collins, K. D. Ions from the Hofmeister Series and Osmolytes: Effects on Proteins in Solution and in the Crystallization Process. *Macromol. Cryst.* **2004**, *34* (3), 300–311.
- Collins, K. D. Ion Hydration: Implications for Cellular Function, Polyelectrolytes, and Protein Crystallization. *Biophys. Chem.* **2006**, *119* (3), 271–281.
- Burghoff, B. Foam Fractionation Applications. *J. Biotechnol.* **2012**, *161* (2), 126–137.
- Lockwood, C. E.; Bummer, P. M.; Jay, M. Purification of Proteins Using Foam Fractionation. *Pharm. Res.* **1997**, *14* (11), 1511–1515.
- Aguilera, J. M.; Lillford, P. J. *Food Materials Science: Principles and Practice*; Springer Science: New York, 2008; p 616.
- Engelhardt, K.; Lexis, M.; Gochev, G.; Konnerth, C.; Miller, R.; Willenbacher, N.; Peukert, W.; Braunschweig, B. Ph Effects on the Molecular Structure of B-Lactoglobulin Modified Air–Water Interfaces and Its Impact on Foam Rheology. *Langmuir* **2013**, *29* (37), 11646–11655.
- Engelhardt, K.; Rumpel, A.; Walter, J.; Domrowski, J.; Kulozik, U.; Braunschweig, B.; Peukert, W. Protein Adsorption at the Electrified

- Air–Water Interface: Implications on Foam Stability. *Langmuir* **2012**, *28* (20), 7780–7787.
- (11) Rosenlehner, K.; Schade, B.; Böttcher, C.; Jäger, C. M.; Clark, T.; Heinemann, F. W.; Hirsch, A. Sodium Effect on Self-Organization of Amphiphilic Carboxylates: Formation of Structured Micelles and Superlattices. *Chem.—Eur. J.* **2010**, *16* (31), 9544–9554.
- (12) Hofmeister, F. Zur Lehre Von Der Wirkung Der Salze. Zweite Mittheilung. *Arch. Exp. Pathol. Pharmakol.* **1888**, *24*, 247–260.
- (13) Kunz, W.; Lo Nostro, P.; Ninham, B. W. The Present State of Affairs with Hofmeister Effects. *Curr. Opin. Colloid Interface Sci.* **2004**, *9* (1–2), 1–18.
- (14) Kunz, W.; Henle, J.; Ninham, B. W. ‘Zur Lehre Von Der Wirkung Der Salze’ (About the Science of the Effect of Salts): Franz Hofmeister’s Historical Papers. *Curr. Opin. Colloid Interface Sci.* **2004**, *9* (1–2), 19–37.
- (15) Jungwirth, P.; Cremer, P. S. Beyond Hofmeister. *Nat. Chem.* **2014**, *6* (4), 261–263.
- (16) Jungwirth, P. Ions at Biological Interfaces. In *Encyclopedia of Applied Electrochemistry*; Springer: Berlin, 2014; p 1131.
- (17) Jungwirth, P. Hofmeister Series of Ions: A Simple Theory of a Not So Simple Reality. *J. Phys. Chem. Lett.* **2013**, *4* (24), 4258–4259.
- (18) Kunz, W. Specific Ion Effects in Colloidal and Biological Systems. *Curr. Opin. Colloid Interface Sci.* **2010**, *15* (1–2), 34–39.
- (19) Gregersen, N.; Bross, P.; Vang, S.; Christensen, J. H. Protein Misfolding and Human Disease. *Annu. Rev. Genomics Hum. Genet.* **2006**, *7* (1), 103–124.
- (20) Tsai, C.-J.; Lin, S. L.; Wolfson, H. J.; Nussinov, R. Studies of Protein-Protein Interfaces: A Statistical Analysis of the Hydrophobic Effect. *Protein Sci.* **1997**, *6* (1), 53–64.
- (21) Beierlein, F. R.; Othersen, O. G.; Lanig, H.; Schneider, S.; Clark, T. Simulating Fret from Tryptophan: Is the Rotamer Model Correct? *J. Am. Chem. Soc.* **2006**, *128* (15), 5142–5152.
- (22) Jäger, C. M.; Hirsch, A.; Schade, B.; Ludwig, K.; Böttcher, C.; Clark, T. Self-Assembly of Structurally Persistent Micelles Is Controlled by Specific-Ion Effects and Hydrophobic Guests. *Langmuir* **2009**, *26* (13), 10460–10466.
- (23) Beierlein, F. R.; Krause, A. M.; Jäger, C. M.; Fita, P.; Vauthery, E.; Clark, T. Molecular Dynamics Simulations of Liquid Phase Interfaces: Understanding the Structure of the Glycerol/Water–Dodecane System. *Langmuir* **2013**, *29* (38), 11898–11907.
- (24) Kirkwood, J. G. Statistical Mechanics of Fluid Mixtures. *J. Chem. Phys.* **1935**, *3* (5), 300–313.
- (25) Michel, J.; Essex, J. Prediction of Protein–Ligand Binding Affinity by Free Energy Simulations: Assumptions, Pitfalls and Expectations. *J. Comput.-Aided Mol. Des.* **2010**, *24* (8), 639–658.
- (26) Michel, J.; Foloppe, N.; Essex, J. W. Rigorous Free Energy Calculations in Structure-Based Drug Design. *Mol. Inf.* **2010**, *29* (8–9), 570–578.
- (27) Gilson, M. K.; Zhou, H.-X. Calculation of Protein-Ligand Binding Affinities. *Annu. Rev. Biophys. Biomol. Struct.* **2007**, *36* (1), 21–42.
- (28) Beierlein, F. R.; Kneale, G. G.; Clark, T. Predicting the Effects of Basepair Mutations in DNA-Protein Complexes by Thermodynamic Integration. *Biophys. J.* **2011**, *101* (5), 1130–1138.
- (29) Beierlein, F. R.; Michel, J.; Essex, J. W. A Simple QM/MM Approach for Capturing Polarization Effects in Protein-Ligand Binding Free Energy Calculations. *J. Phys. Chem. B* **2011**, *115*, 4911–4926.
- (30) Wong, D. W. S.; Camirand, W. M.; Pavlath, A. E. Structures and Functionalities of Milk Proteins. *Crit. Rev. Food Sci. Nutr.* **1996**, *36*, 807–844.
- (31) Verheul, M.; Pedersen, J. S.; Roefs, S. P. F. M.; de Kruif, K. G. Association Behavior of Native B-Lactoglobulin. *Biopolymers* **1999**, *49* (1), 11–20.
- (32) Gebhardt, R.; Toro-Sierra, J.; Kulozik, U. Pressure Dissociation of [Small Beta]-Lactoglobulin Oligomers near Their Isoelectric Point. *Soft Matter* **2012**, *8* (46), 11654–11660.
- (33) Bromley, E. H. C.; Krebs, M. R. H.; Donald, A. M. Aggregation across the Length-Scales in [Small Beta]-Lactoglobulin. *Faraday Discuss.* **2005**, *128* (0), 13–27.
- (34) Bromley, E. H. C.; Krebs, M. R. H.; Donald, A. M. Mechanisms of Structure Formation in Particulate Gels of B-Lactoglobulin Formed near the Isoelectric Point. *Eur. Phys. J. E* **2006**, *21* (2), 145–152.
- (35) Krebs, M. R. H.; Bromley, E. H. C.; Donald, A. M. The Binding of Thioflavin-T to Amyloid Fibrils: Localisation and Implications. *J. Struct. Biol.* **2005**, *149* (1), 30–37.
- (36) Qin, B. Y.; Bewley, M. C.; Creamer, L. K.; Baker, H. M.; Baker, E. N.; Jameson, G. B. Structural Basis of the Tanford Transition of Bovine B-Lactoglobulin. *Biochemistry* **1998**, *37* (40), 14014–14023.
- (37) Tanford, C.; Bunville, L. G.; Nozaki, Y. The Reversible Transformation of B-Lactoglobulin at pH 7.51. *J. Am. Chem. Soc.* **1959**, *81* (15), 4032–4036.
- (38) Majhi, P. R.; Ganta, R. R.; Vanam, R. P.; Seyrek, E.; Giger, K.; Dubin, P. L. Electrostatically Driven Protein Aggregation: B-Lactoglobulin at Low Ionic Strength. *Langmuir* **2006**, *22* (22), 9150–9159.
- (39) Guex, N.; Peitsch, M. C. Swiss-Model and the Swiss-Pdbviewer: An Environment for Comparative Protein Modeling. *Electrophoresis* **1997**, *18*, 2714–2723.
- (40) Persistence of Vision Raytracer, version 3.6; Persistence of Vision Pty. Ltd.: Williamstown, Victoria, Australia, 2004.
- (41) Engelhardt, K.; Peukert, W.; Braunschweig, B. Vibrational Sum-Frequency Generation at Protein Modified Air-Water Interfaces: Effects of Molecular Structure and Surface Charging. *Curr. Opin. Colloid Interface Sci.* **2014**, *19* (3), 207–215.
- (42) Bonn, M.; Bakker, H.; Tong, Y.; Backus, E. H. G. No Ice-Like Water at Aqueous Biological Interfaces. *Biointerphases* **2012**, *7* (1–4), 1–5.
- (43) Zhang, C.; Jasensky, J.; Leng, C.; Gross, C. D.; Smith, G. D.; Wilker, J. J.; Chen, Z. Sum Frequency Generation Vibrational Spectroscopic Studies on Buried Heterogeneous Biointerfaces. *Opt. Lett.* **2014**, *39* (9), 2715–2718.
- (44) Anandakrishnan, R.; Aguilar, B.; Onufriev, A. V. H++ 3.0: Automating Pk Prediction and the Preparation of Biomolecular Structures for Atomistic Molecular Modeling and Simulations. *Nucleic Acids Res.* **2012**, *40* (W1), W537–W541.
- (45) Myers, J.; Grothaus, G.; Narayanan, S.; Onufriev, A. A Simple Clustering Algorithm Can Be Accurate Enough for Use in Calculations of Pks in Macromolecules. *Proteins: Struct., Funct., Bioinf.* **2006**, *63* (4), 928–938.
- (46) Gordon, J. C.; Myers, J. B.; Folta, T.; Shoja, V.; Heath, L. S.; Onufriev, A. H++: A Server for Estimating PkAs and Adding Missing Hydrogens to Macromolecules. *Nucleic Acids Res.* **2005**, *33* (Suppl. 2), W368–W371.
- (47) Li, H.; Robertson, A. D.; Jensen, J. H. Very Fast Empirical Prediction and Rationalization of Protein Pka Values. *Proteins: Struct., Funct., Bioinf.* **2005**, *61* (4), 704–721.
- (48) Bas, D. C.; Rogers, D. M.; Jensen, J. H. Very Fast Prediction and Rationalization of Pka Values for Protein–Ligand Complexes. *Proteins: Struct., Funct., Bioinf.* **2008**, *73* (3), 765–783.
- (49) Olsson, M. H. M.; Søndergaard, C. R.; Rostkowski, M.; Jensen, J. H. Propka3: Consistent Treatment of Internal and Surface Residues in Empirical Pka Predictions. *J. Chem. Theory Comput.* **2011**, *7* (2), 525–537.
- (50) Søndergaard, C. R.; Olsson, M. H. M.; Rostkowski, M.; Jensen, J. H. Improved Treatment of Ligands and Coupling Effects in Empirical Calculation and Rationalization of Pka Values. *J. Chem. Theory Comput.* **2011**, *7* (7), 2284–2295.
- (51) Vriend, G. What If: A Molecular Modeling and Drug Design Program. *J. Mol. Graphics* **1990**, *8*, 52–56.
- (52) Bernstein, F. C.; Koetzle, T. F.; Williams, G. J. B.; Meyer, E. F., Jr.; Brice, M. D.; Rodgers, J. R.; Kennard, O.; Shimanouchi, T.; Tasumi, M. The Protein Data Bank: A Computer-Based Archival File for Macromolecular Structures. *J. Mol. Biol.* **1977**, *112*, 535–542.
- (53) Berman, H. M.; Westbrook, J.; Feng, Z.; Gilliland, G.; Bhat, T. N.; Weissig, H.; Shindyalov, I. N.; Bourne, P. E. The Protein Data Bank. *Nucleic Acids Res.* **2000**, *28*, 235–242.

- (54) Case, D. A.; Darden, T. A.; Cheatham, T. E., III; Simmerling, C. L.; Wang, J.; Duke, R. E.; Luo, R.; Walker, R. C.; Zhang, W.; Merz, K. M.; et al. *Amber 12*; University of California: San Francisco, CA, 2012.
- (55) Berendsen, H. J. C.; Grigera, J. R.; Straatsma, T. P. The Missing Term in Effective Pair Potentials. *J. Phys. Chem.* **1987**, *91* (24), 6269–6271.
- (56) Joung, I. S.; Cheatham, T. E., III. Determination of Alkali and Halide Monovalent Ion Parameters for Use in Explicitly Solvated Biomolecular Simulations. *J. Phys. Chem. B* **2008**, *112* (30), 9020–9041.
- (57) Roe, D. R.; Cheatham, T. E. PTRAJ and CPPTRAJ: Software for Processing and Analysis of Molecular Dynamics Trajectory Data. *J. Chem. Theory Comput.* **2013**, *9* (7), 3084–3095.
- (58) Jäger, C. M.; Hirsch, A.; Schade, B.; Ludwig, K.; Böttcher, C.; Clark, T. Self-Assembly of Structurally Persistent Micelles Is Controlled by Specific-Ion Effects and Hydrophobic Guests. *Langmuir* **2010**, *26* (13), 10460–10466.
- (59) Jäger, C. M.; Hirsch, A.; Schade, B.; Böttcher, C.; Clark, T. Counterions Control the Self-Assembly of Structurally Persistent Micelles: Theoretical Prediction and Experimental Observation of Stabilization by Sodium Ions. *Chem.—Eur. J.* **2009**, *15* (34), 8586–8592.
- (60) Steinbrecher, T.; Mobley, D. L.; Case, D. A. Nonlinear Scaling Schemes for Lennard-Jones Interactions in Free Energy Calculations. *J. Chem. Phys.* **2007**, *127* (21), 214108.
- (61) Steinbrecher, T.; Joung, I.; Case, D. A. Soft-Core Potentials in Thermodynamic Integration: Comparing One- and Two-Step Transformations. *J. Comput. Chem.* **2011**, *32* (15), 3253–3263.
- (62) Marrink, S. J.; Risselada, H. J.; Yefimov, S.; Tieleman, D. P.; de Vries, A. H. The Martini Force Field: Coarse Grained Model for Biomolecular Simulations. *J. Phys. Chem. B* **2007**, *111* (27), 7812–7824.
- (63) Monticelli, L.; Kandasamy, S. K.; Periole, X.; Larson, R. G.; Tieleman, D. P.; Marrink, S.-J. The Martini Coarse-Grained Force Field: Extension to Proteins. *J. Chem. Theory Comput.* **2008**, *4* (5), 819–834.
- (64) de Jong, D. H.; Singh, G.; Bennett, W. F. D.; Arnarez, C.; Wassenaar, T. A.; Schäfer, L. V.; Periole, X.; Tieleman, D. P.; Marrink, S. J. Improved Parameters for the Martini Coarse-Grained Protein Force Field. *J. Chem. Theory Comput.* **2013**, *9* (1), 687–697.
- (65) Richmond, G. L. Molecular Bonding and Interactions at Aqueous Surfaces as Probed by Vibrational Sum Frequency Spectroscopy. *Chem. Rev.* **2002**, *102* (8), 2693–2724.
- (66) Shen, Y. R.; Ostroverkhov, V. Sum-Frequency Vibrational Spectroscopy on Water Interfaces: Polar Orientation of Water Molecules at Interfaces: Chemical Reviews. *Chem. Rev.* **2006**, *106* (4), 1140–1154.
- (67) Gragson, D. E.; Richmond, G. L. Investigations of the Structure and Hydrogen Bonding of Water Molecules at Liquid Surfaces by Vibrational Sum Frequency Spectroscopy: The Journal of Physical Chemistry B. *J. Phys. Chem. B* **1998**, *102* (20), 3847–3861.
- (68) Sovago, M.; Campen, R. K.; Wurpel, G. W. H.; Müller, M.; Bakker, H. J.; Bonn, M. Vibrational Response of Hydrogen-Bonded Interfacial Water Is Dominated by Intramolecular Coupling. *Phys. Rev. Lett.* **2008**, *100* (17), 173901.
- (69) Wang, J.; Buck, S. M.; Chen, Z. Sum Frequency Generation Vibrational Spectroscopy Studies on Protein Adsorption. *J. Phys. Chem. B* **2002**, *106* (44), 11666–11672.
- (70) Perriman, A. W.; Henderson, M. J.; Holt, S. A.; White, J. W. Effect of the Air–Water Interface on the Stability of B-Lactoglobulin. *J. Phys. Chem. B* **2007**, *111* (48), 13527–13537.
- (71) Marsh, R. J.; Jones, R. A. L.; Sferrazza, M.; Penfold, J. Neutron Reflectivity Study of the Adsorption of B-Lactoglobulin at a Hydrophilic Solid/Liquid Interface. *J. Colloid Interface Sci.* **1999**, *218* (1), 347–349.
- (72) Beretta, S.; Chirico, G.; Baldini, G. Short-Range Interactions of Globular Proteins at High Ionic Strengths. *Macromolecules* **2000**, *33* (23), 8663–8670.
- (73) Timasheff, S. N.; Mescanti, L.; Basch, J. J.; Townend, R. Conformational Transitions of Bovine B-Lactoglobulins a, B, and C. *J. Biol. Chem.* **1966**, *241* (11), 2496–2501.
- (74) Humphrey, W.; Dalke, A.; Schulten, K. VMD - Visual Molecular Dynamics. *J. Mol. Graphics* **1996**, *14*, 33–38.
- (75) Jungwirth, P. Spiers Memorial Lecture Ions at Aqueous Interfaces. *Faraday Discuss.* **2009**, *141* (0), 9–30.
- (76) Kubíčková, A.; Křížek, T.; Coufal, P.; Vazdar, M.; Wernersson, E.; Heyda, J.; Jungwirth, P. Overcharging in Biological Systems: Reversal of Electrophoretic Mobility of Aqueous Polyaspartate by Multivalent Cations. *Phys. Rev. Lett.* **2012**, *108* (18), 186101.
- (77) Vrbka, L.; Vondrášek, J.; Jagoda-Cwiklik, B.; Vácha, R.; Jungwirth, P. Quantification and Rationalization of the Higher Affinity of Sodium over Potassium to Protein Surfaces. *Proc. Natl. Acad. Sci. U. S. A.* **2006**, *103* (42), 15440–15444.
- (78) Jagoda-Cwiklik, B.; Vácha, R.; Lund, M.; Srebro, M.; Jungwirth, P. Ion Pairing as a Possible Clue for Discriminating between Sodium and Potassium in Biological and Other Complex Environments. *J. Phys. Chem. B* **2007**, *111* (51), 14077–14079.
- (79) Štěpánková, V.; Paterová, J.; Damborský, J.; Jungwirth, P.; Chaloupková, R.; Heyda, J. Cation-Specific Effects on Enzymatic Catalysis Driven by Interactions at the Tunnel Mouth. *J. Phys. Chem. B* **2013**, *117* (21), 6394–6402.
- (80) Kherb, J.; Flores, S. C.; Cremer, P. S. Role of Carboxylate Side Chains in the Cation Hofmeister Series. *J. Phys. Chem. B* **2012**, *116* (25), 7389–7397.
- (81) Hess, B.; van der Vegt, N. F. A. Cation Specific Binding with Protein Surface Charges. *Proc. Natl. Acad. Sci. U. S. A.* **2009**, *106* (32), 13296–13300.
- (82) Paterová, J.; Rembert, K. B.; Heyda, J.; Kurra, Y.; Okur, H. I.; Liu, W. R.; Hilty, C.; Cremer, P. S.; Jungwirth, P. Reversal of the Hofmeister Series: Specific Ion Effects on Peptides. *J. Phys. Chem. B* **2013**, *117* (27), 8150–8158.
- (83) Heyda, J.; Hrobárik, T.; Jungwirth, P. Ion-Specific Interactions between Halides and Basic Amino Acids in Water. *J. Phys. Chem. A* **2009**, *113* (10), 1969–1975.
- (84) Vrbka, L.; Jungwirth, P.; Bauduin, P.; Touraud, D.; Kunz, W. Specific Ion Effects at Protein Surfaces: A Molecular Dynamics Study of Bovine Pancreatic Trypsin Inhibitor and Horseradish Peroxidase in Selected Salt Solutions. *J. Phys. Chem. B* **2006**, *110* (13), 7036–7043.
- (85) Swails, J. M.; York, D. M.; Roitberg, A. E. Constant Ph Replica Exchange Molecular Dynamics in Explicit Solvent Using Discrete Protonation States: Implementation, Testing, and Validation. *J. Chem. Theory Comput.* **2014**, *10* (3), 1341–1352.
- (86) Mongan, J.; Case, D. A.; McCammon, J. A. Constant Ph Molecular Dynamics in Generalized Born Implicit Solvent. *J. Comput. Chem.* **2004**, *25* (16), 2038–2048.
- (87) Hennemann, M.; Clark, T. Empire: A Highly Parallel Semiempirical Molecular Orbital Program: 1: Self-Consistent Field Calculations. *J. Mol. Model.* **2014**, *20* (7), 1–11.
- (88) Clark, T.; Chandrasekhar, J. NDDO-Based CI Methods for the Prediction of Electronic Spectra and Sum-over-States Molecular Hyperpolarization. *Isr. J. Chem.* **1993**, *33*, 435–448.
- (89) Göller, A.; Grummt, U.-W. Implementation of an NDDO/Ci/SOS Approach for Second-Order Hyperpolarizabilities. *Int. J. Quantum Chem.* **2000**, *77* (4), 727–760.